Available online at www.sciencedirect.com
ScienceDirect
International Journal of Thermal Sciences 48 (2009) 761–772
International Journal of Thermal Sciences
www.elsevier.com/locate/ijts

Laser pulse heating and phase changes in the irradiated region: Temperature-dependent thermal properties case

B.S. Yilbas *, S.B. Mansoor

Mechanical Engineering Department, KFUPM Box 1913, Dhahran 31261, Saudi Arabia

Received 2 November 2007; received in revised form 21 May 2008; accepted 21 May 2008

Available online 26 June 2008

Abstract

Laser heating and phase change processes in the substrate material are formulated using the energy method. Constant and temperature-dependent thermal properties (variable thermal properties) of the substrate material are considered in the simulations for comparison. Temperature rise in the substrate material and mushy zones formed across liquid–solid and liquid–vapor phases are predicted for constant and variable thermal properties cases. Laser pulse intensity resembling the actual laser pulse is accommodated in the analysis. The recession velocity predicted from the present simulation is compared with the results of analytical solution obtained previously for constant properties case. The cavity depth predicted is compared with the experimental results. It is found that the simulation for constant properties results in early evaporation of the surface and deeper cavities as compared to variable thermal properties case. The prediction of cavity depth for variable thermal properties case agrees well with the experimental results.

Keywords: Laser; Heating; Phase change; Cavity formation

1. Introduction

High power interaction with a solid substrate results in solid heating of the bulk and consequent melting and evaporation of the irradiated surface. Since the process is fast and involves with high temperature phenomena for the laser short pulses, modeling of the laser–solid interaction process becomes essential. Model studies also provide insight into the physical processes taking place during the course of interaction. Moreover, when modeling of such physical processes, phase change and mushy zone formation across each phase should be considered. Although the mushy zone generated between the co-existed phases is small in size, the consideration of the mushy zone is essential to capture the actual physical processes. Since the material properties vary with temperature; therefore, temperature dependent thermophysical properties should be introduced in the simulations.

Considerable research studies were carried out to examine the laser evaporative heating process. Yilbas [1] introduced the analytical solution for the laser evaporative heating process while assuming a thermal equilibrium during the evaporation at the surface. However, the heating situation is three-dimensional and energy transfer in the radial direction should be accounted for. Yilbas et al. [2] examined the steady evaporation rate of the surface analytically for laser machining applications. However, the analysis was limited with co-existing of two phases and mushy zone consideration was neglected in the model study due to the simplicity. Numerical modeling of a laser heating situation was considered by Yilbas [3]. He introduced the surface functions to accommodate for the surface evaporation. However, temporal variation of evaporation rate was limited to the considerable short durations due to the computational difficulties.

A numerical approach for laser heating process in relation to drilling is introduced by Ganesh et al. [4]. They used the flow equations to predict the vapor front behavior during the evaporation process while accommodating the constant properties of the substrate material in the analysis. A mathematical model for the phase change in laser welding of solid substrate was

* Corresponding author.
E-mail address: bsyilbas@kfupm.edu.sa (B.S. Yilbas).

1290-0729/$ – see front matter
doi:10.1016/j.ijthermalsci.2008.05.013

Nomenclature

A	area	m^2
a	Gaussian parameter	m
Cp_m	specific heat capacity of liquid phase	J/kg/K
Cp_s	specific heat capacity of solid phase	J/kg/K
Cp_b	specific heat capacity of vapor phase	J/kg/K
C	various empirical constants in turbulence model	
h	convective heat transfer coefficient	$W/m^2/K$
	sensible enthalpy	J/kg
I_o	laser power intensity	W/m^2
k	thermal conductivity	W/m/K
k_m	thermal conductivity of liquid phase	W/m/K
k_s	thermal conductivity of solid phase	W/m/K
k_b	thermal conductivity of vapor phase	W/m/K
L_m	latent heat of melting	J/kg
L_v	latent heat of evaporation	J/kg
r	distance along the radial direction	m
r_f	reflectance	
S	source term	W/m^3
T	temperature	K
T_m	melting temperature	K
T_b	evaporation temperature	K
t_m	time at which melting starts in the solid phase	s
t_{sl}	time at which solid-liquid mushy zone starts converting into the liquid phase	s
t_b	time at which evaporation starts in the liquid phase	s
U	energy content	J
$\forall$	volume	m^3
x	quality	
zc	depth of cavity	m
z	distance along the radial direction	m

Greek symbols

δ	reciprocal of absorption depth	m^{-1}
ρ	density	kg/m^3

Subscripts

b	vapor–liquid mushy zone; vapor
m	liquid–solid mushy zone liquid
max	maximum; maximum cavity radius
ref	reference
s	solid, surface

introduced by Pecharapa and Kar [5]. They developed simplified expression for the shapes of the solid–liquid and liquid–vapor interfaces during the quasi-steady state heating situation. Laser ablation of solid surface and numerical simulation of vapor front was carried out by Liu et al. [6]. They assumed the equation of state for a vapor phase in a simplified form and one-dimensional gas dynamic equations were accommodated in the analysis. The semi-analytical approach for laser drilling of metals was presented by Solana et al. [7]. They used a perturbation technique for temporal solution of the vaporization process after the assumption of constant material properties. Two-dimensional gas dynamic model for the laser ablation was introduced by Gusarov et al. [8]. However, the solid heating and phase change processes were modeled in one-dimensional form. The laser alloying of metallic surfaces using a laser was examined by Kim and Sim [9]. They indicated that mushy zone developed between solid–liquid interface had significant effect on the heat transfer rates from liquid metal to the solid bulk. Temperature calculation in the melt during laser heating process was carried out by Rostami and Raisi [10]. They showed that the heat affected zone increased with increasing workpiece transition speed. Laser key-hole formation during laser deep penetration welding was formulated by Matsunawa and Semak [11]. They showed that humps on the key hole occurred when the speed of melt isotherms became higher than the translational speed. Laser evaporative heating of metallic surfaces was investigated by Zhang and Faghri [12]. They indicated that increasing conduction losses from the melt zone reduced significantly the liquid layer thickness. Laser melting process and flow circulation in the melt pool was investigated by Basu and Date [13]. They predicted numerically temperature distribution in the melt pool and obtained the mushy zone across the solid and liquid phases using the enthalpy method. Shen et al. [14] investigated the laser induced heating and melting in solids. They developed the expression for the melt depth after assuming temperature profiles in the liquid and solid regions. The numerical analysis of the effects of non-conventional laser beam geometries during laser melting of metallic materials was carried out by Safdar et al. [15]. They predicted the sizes of melt and mushy zones after considering the surface heat source heating situation. The enthalpy-based lattice Boltzmann model for diffusion dominated solid–liquid phase transformation was introduced by Chatterjee and Chakraborty [16]. The proposed model provided temperature predictions in the melt, mushy, and solid zones for the constant properties case and the surface heat flux heating situation. Yilbas and Mansour [17] cavity formation and vapor jet expansion from the cavity. They showed that the vapor pressure close to 1 GPa occurred in the cavity for the short heating duration. Bin Mansoor and Yilbas [18] considered the laser induced evaporation process and predicted the surface recession numerically for constant material properties. However, the material properties are temperature dependent and should be accommodated in the analysis to secure the accurate results.

In the present study, an extension of the previous work [18], laser non-conduction limited heating of steel surface is considered and phase change processes due to melting and evaporation are modeled using the energy method. Temperature dependent thermal properties are accommodated in the analysis and predictions due to the constant properties are compared with their counterparts corresponding to the variable thermal properties. The laser pulse used in the simulation resembles the actual laser pulse used in the experiment. The predictions of recession velocity and laser produced cavity depth are compared with the

previous analytical solutions [19] and experimental results, respectively.

2. Mathematical analysis

Energy equation for each phase is solved independently as well as being coupled across the interfaces of the two-phases, where both phases exist mutually (mushy zones). In the case of constant properties, governing equations of heat transfer and mushy zone are solved numerically while assuming all the thermal properties are constant. The laser output power intensity distribution at the workpiece surface is considered being Gaussian and its centre is located at the centre of the co-ordinate system. The temporal variation of laser power intensity resembling the actual laser pulse is accommodated in the simulations. This arrangement results in an axisymmetric heating of the workpiece material. The heat conduction equation for a solid phase heating due to a laser irradiation pulse with a Gaussian intensity profile can be written as:

$$\frac{\partial}{\partial t}(\rho_s c_{p_s} T) = \frac{1}{r}\frac{\partial}{\partial r}\left(k_s r \frac{\partial T}{\partial r}\right) + \frac{\partial}{\partial z}\left(k_s \frac{\partial T}{\partial z}\right) + S_o \tag{1}$$

where S_o is the volumetric source term and it is,

$$S_o = I_o \delta (1 - r_f) \exp(-\delta z) \exp\left(-\frac{r^2}{a^2}\right) \tag{2}$$

I_o, δ, r_f and a are the laser peak power intensity, absorption coefficient, reflectivity and the Gaussian parameter, respectively.

The initial and boundary conditions for Eq. (1) are given below. Initially, the substrate material is assumed at a uniform temperature, T_o, i.e.:

at time zero $\Rightarrow$ $t = 0$: $T(r, z, 0) = T_o$ (specified)

At a distance considerably away from the surface (at infinity) in the radial direction a constant temperature T_o is assumed. Since the heating has no effect on the temperature rise at a depth of infinity below the surface, temperature is assumed to be constant and equals to the initial temperature of the substrate material in this region. The respective boundary conditions are:

r at infinity $\Rightarrow$ $r = \infty$: $T(\infty, z, t) = T_o$ (specified)

z at infinity $\Rightarrow$ $z = \infty$: $T(r, \infty, t) = T_o$ (specified)

At the symmetry axis, maximum temperature is assumed and the convection boundary condition is considered at the workpiece surface, i.e.:

at symmetry axis $\Rightarrow$ $r = 0$: $\dfrac{\partial T(0, z, t)}{\partial r} = 0$

and

at the surface $\Rightarrow$ $z = 0$: $k\dfrac{\partial T(r, 0, t)}{\partial z} = h\big(T(r, 0, t) - T_o\big)$

where h is taken as 10 $\mathrm{W/m^2\,K}$ due to natural convection from the surface prior to evaporation [20].

Since the evaporation temperature depends on the pressure and this relation is not known for steel vapor, it is assumed that the substrate material has single melting and boiling temperatures. Moreover, once the phase change initiates, a mushy zone (mutually existence of two-phases) is introduced across the interface of two phases (Fig. 1). During the phase change process, including the mushy zone, temperature of the substrate material remains the same, but its enthalpy changes in this region. This situation can be formulated via energy balance in the mushy zone. It should be noted that nominal laser pulse length is 24 ns, therefore, the flow in the vapor and liquid layer during the heating process is neglected, i.e. 1 μm of fluid motion, in radial or axial direction, in the liquid layer requires the liquid velocity in the order of 1000 m/s, which may not be the case that occurs in the present simulations; consequently, during the short heating period, the fluid motion in the liquid and vapor layers is assumed not to influence the heat transfer mechanism in these zones. Consider a differential element in the mushy zone (Fig. 1) and let x_m is the mass fraction of liquid present in the element. Energy content (ΔU) of the differential element with volume $\Delta\forall$ at melting temperature T_m can be written as:

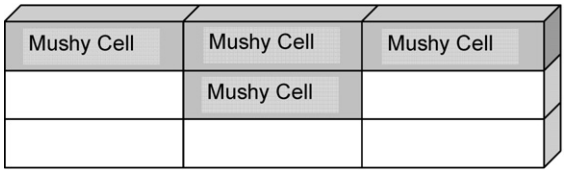

Fig. 1. A schematic view of the mushy zone.

$$\Delta U = \rho_m \Delta\forall\big[x_m\big(L_m + c_{p_m}(T_m - T_{\mathrm{ref}})\big) + c_{p_s}(1 - x_m)(T_m - T_{\mathrm{ref}})\big] \tag{3}$$

where

$$x_m = \frac{m_m}{m_m + m_s}$$

$T_{\mathrm{ref}}, x_m, m_m, m_s$ are reference temperature for enthalpy, quality (mass fraction) of liquid, mass of liquid and mass of solid in the element, respectively. After assuming specific heat of melt is the same as the solid at the melting temperature ($c_{p_s} = c_{p_m}$ at $T = T_m$), and differentiation of Eq. (3) with time yields:

$$\frac{\partial u}{\partial t} = \rho_m L_m \frac{\partial x_m}{\partial t} \tag{4}$$

since $c_{p_m}(T_m - T_{\mathrm{ref}}) = \text{const.}$ and $u = \frac{U}{\forall}$.

Substituting Eq. (4) into Eq. (1) and re-arrangement results the energy equation for the differential element in the mushy zone:

$$\rho_m L_m \frac{\partial x_m}{\partial t} = \frac{1}{r}\frac{\partial}{\partial r}\left(k_m r \frac{\partial T}{\partial r}\right) + \frac{\partial}{\partial z}\left(k_m \frac{\partial T}{\partial z}\right) + S_o \tag{5}$$

Eq. (5) is valid in the mushy zone where$0 \leqslant x_m \leqslant 1$, i.e. temperature of the cells with $0 \leqslant x_m \leqslant 1$ is set to melting temperature ($T = T_m$). For the situation $x_m = 1$, liquid phase occurs and Eq. (1) is used to determine the temperature rise in the liquid heating with using the liquid thermal properties in the equation. Moreover, the liquid heating continues until the boiling point is reached in the substrate material; in which case, a new mushy zone is formed. In this case, Eq. (5) is modified for a differential element in the mushy zone subjected to evaporation, i.e.:

$$\rho_b L_b \frac{\partial x_b}{\partial t} = \frac{1}{r}\frac{\partial}{\partial r}\left(k_b r \frac{\partial T}{\partial r}\right) + \frac{\partial}{\partial z}\left(k_b \frac{\partial T}{\partial z}\right) + S_o \tag{6}$$

Table 1
Thermal properties of substrate material and pulse parameters used in the simulations

k_s	$139.7356-(0.1896)T+(0.0001)T^2$ (W/m K) (solid phase)
ρ_s	7860 (Kg/m^3) (solid phase)
Cp_s	$110.0215+(1.2405)T-(0.0006)T^2$ (J/kg K) (solid phase)
K_m	37 (W/m K) (liquid phase)
ρ_m	6891 7860 (Kg/m^3) (liquid phase)
Cp_m	824 (J/kg K) (liquid phase)
K_b	$(0.9)k_m$ (W/m K) (vapor phase)
ρ_b	$\rho_m/15$ (Kg/m^3) (vapor phase)
Cp_b	$(1.1)Cp_m$ (vapor phase)
L_m	247112 (J/kg)
T_m	1811 (K)
L_b	6213627 (J/kg)
T_b	3134 (K)
T_o	300 (K)
T_∞	300 (K)
δ	6.17×10^6 (1/m)
r_f	0.5
r_o	1.25×10^{-5} (m)
a	$2r_o/3$ (m)
I_o	5×10^{12} (W/m^2)
I	$I_o\delta\exp(-\delta z)\exp\left(\left(-\frac{r}{a}\right)^2\right)\left(0.01057\left(\frac{t}{2.71\times10^{-8}}\right)+0.01182\left(\frac{t}{2.71\times10^{-8}}\right)^2+750.00438\left(\frac{t}{2.71\times10^{-8}}\right)^3\right)\exp\left(-10.11068\left(\frac{t}{2.71\times10^{-8}}\right)\right)$
Nominal pulse length	24 (ns)

Eq. (6) is applicable for temperature $T=T_b$ and $0\leqslant x_b\leqslant 1$ in the mushy zone (partially liquid partially vapor zone); in which case, temperature of the cells with $0\leqslant x_b\leqslant 1$ is set to the boiling temperature of the substrate material($T=T_b$). It should be noted that x_m is replaced with $x_b$in Eq. (5), which represents the fraction of vapor phase in the differential element. The calculation of x_b is the same as x_m, provided that latent heat of fusion is replaced with latent heat of evaporation of the substrate material in Eq. (5) in the later.

The boundary condition at the evaporating surface is introduced in relation to Eq. (6). In this case, the temperature along the evaporated surface is kept at boiling temperature of the substrate material, i.e., the cells in the evaporated region are kept at boiling temperature, i.e.:

In the mushy zone, at $z=z_b\Rightarrow T(r,z_b,t)=T_b$ where z_b represents the axial location at the evaporated surface.

Eqs. (5) and (6) provide the relative position of solid–liquid and liquid–vapor interface in the substrate material. Liquid–vapor interface determines the shape and size of the cavity generated during evaporation process.

3. Numerical solution

Eq. (1) is applicable to solid and liquid heating, Eq. (5) is applicable to mushy zone at solid–liquid interface and Eq. (6) is applicable to mushy zone at liquid–vapor interface. To discretize the governing equations, a finite difference scheme is introduced. The details of the numerical scheme are given in [21]. To compute the equations discretized for temperature field and relative positions of solid–liquid and liquid–vapor interface, an implicit scheme is used, i.e. using the initial conditions, the temperature in the whole domain is calculated for following time steps with the respective conditions. The discretization procedure is given in the appendix. The temporal resolution for the implicit scheme is set as 0.5×10^{-9} s in the simulations.

The calculation domain is divided into the staggered grids and the grid independence test is performed for the different grid sizes and orientations. The grid size resulting the grid independent solution is used in the simulations, i.e., the grid containing 100×120 mesh points in the r and z-axes is accommodated. In the z-axis, a spacing of $\Delta z=3.2415\times10^{-8}$ m is used while in the radial direction (normal to the laser beam axis) $\Delta r=8.3333\times10^{-8}$ m increment is selected. A computer program employing the implicit scheme is developed to compute the temperature field and the relative positions of solid–liquid and liquid–vapor interfaces. Since the first-order backward differences for time derivatives are used, the discretized equations constitute an implicit scheme. In the absence of convection terms, which is the case in hand, this scheme is unconditionally stable with respect to the size of the time step Δt, given that the spatial steps Δr and Δz are fixed.

The material properties and pulse intensity used in the simulations are given in Table 1. It should be noted that the laser pulse properties employed in the simulations resemble the actual pulse used in the experiment (Fig. 2).

4. Results and discussion

Laser evaporative heating and cavity formation in the solid substrate is modeled. The energy method is used to identify the mushy zones between solid–liquid and liquid–vapor phases. Constant and variable thermal properties of the substrate material are employed in the simulation to examine the influence of the substrate properties on temperature field, formation of the

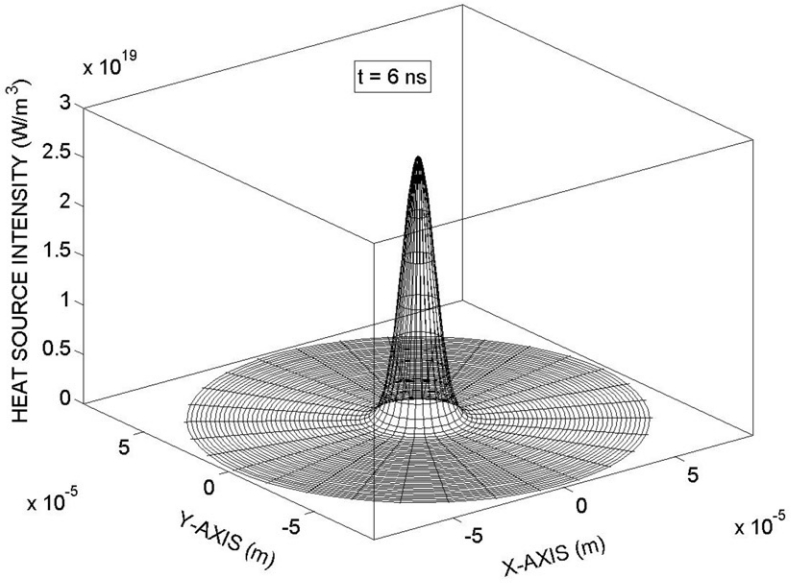

Spatial distribution of laser pulse.

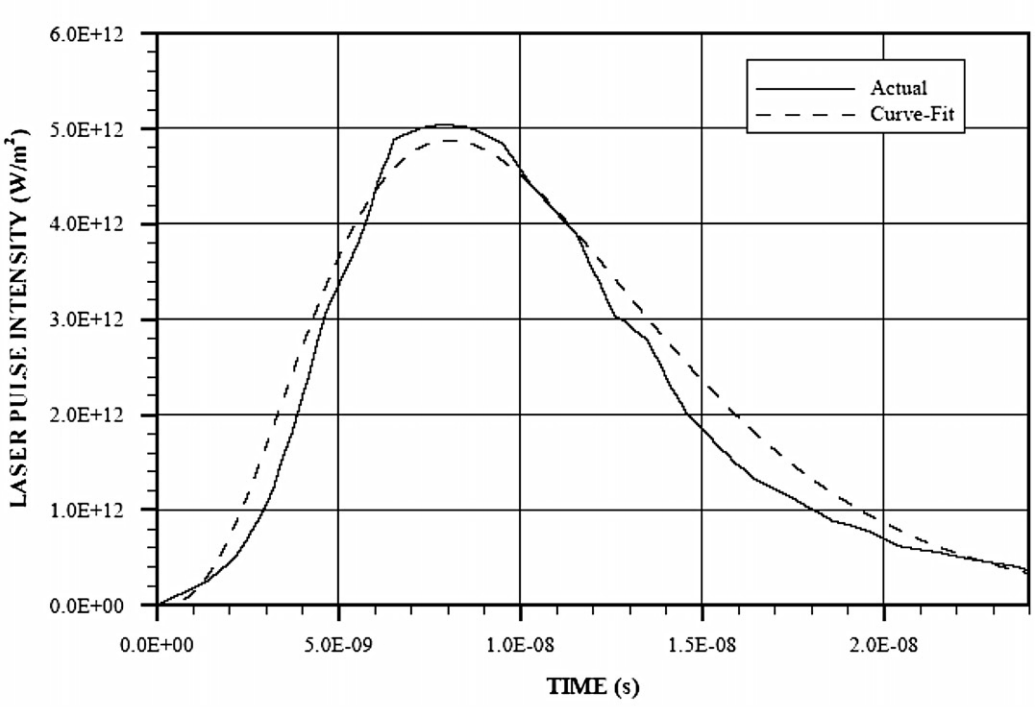

Temporal variation of laser pulse

Fig. 2. Laser pulse intensity used in the simulations.

mushy zones, and the cavity size. Table 1 gives the material properties and laser pulse parameters used in the simulations.

Fig. 3 shows the temperature contours and cavity formation in the surface region of the substrate material during two heating periods and for constant and variable thermal properties of the substrate material. The cavity size enhances particularly in the axial direction for the constant properties case, which is more pronounced in the early heating periods when laser pulse intensity increases with the time. The decrease in cavity depth due to the variable thermal properties case is associated with the decrease in thermal conductivity and increase in specific heat capacity with increasing temperature, i.e., thermal conductivity is 134 W/m/K at 100 °C and 31.2 W/m/K at 1500 °C while specific heat is 216 J/kg K at 100 °C and 654 J/kg K at 1500 °C. In this case, decreasing thermal conductivity results in small heat diffusion from the irradiated region to the solid bulk.

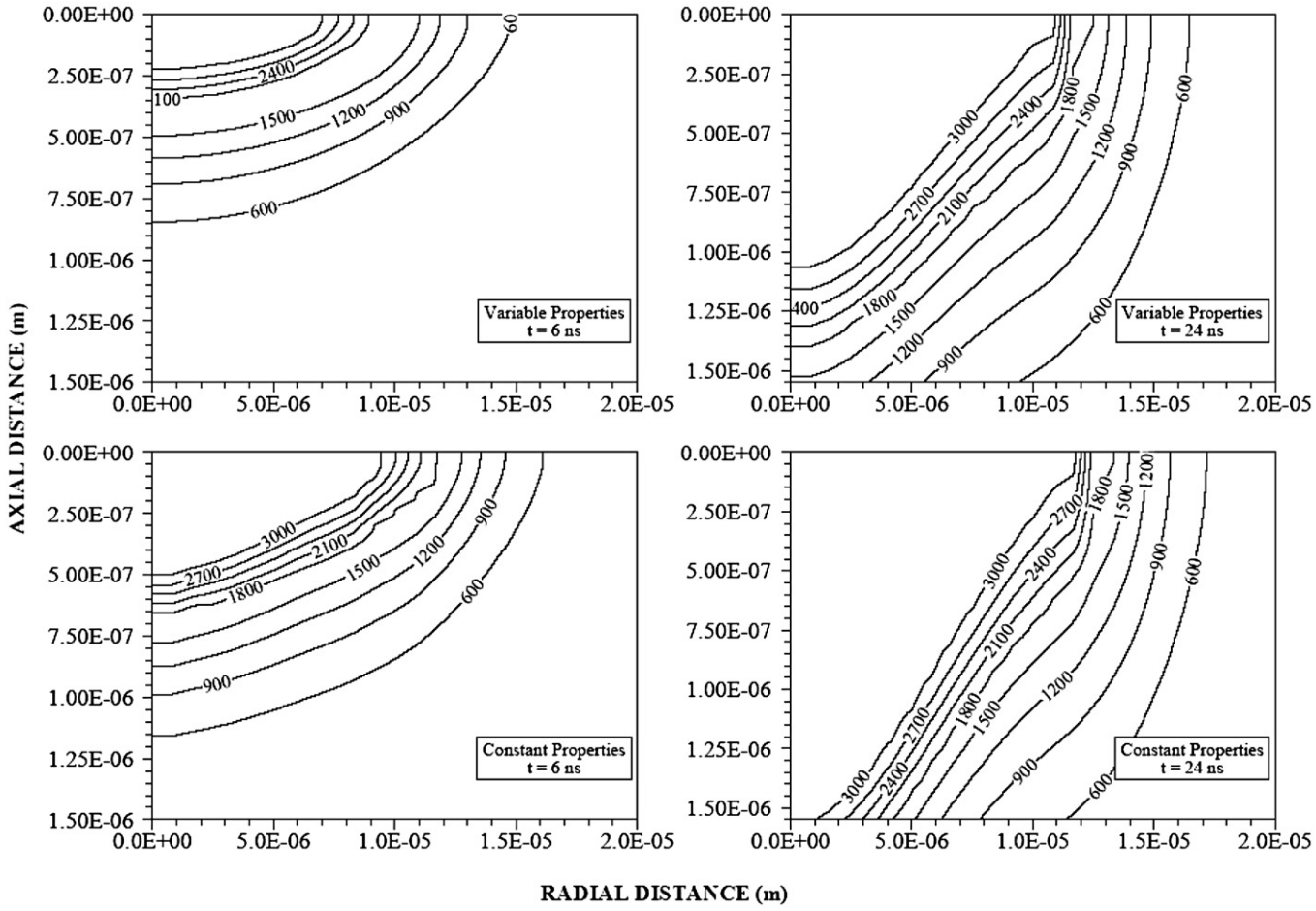

Fig. 3. Temperature counters for constant and variable thermal properties cases.

However, increasing specific heat capacity reduces temperature rise in the irradiated region for the same internal energy gain for both constant and variable thermal properties cases. This, in turn, suppresses the melting and evaporation rates in the surface region. Consequently, cavity depth becomes shallower in the region particularly where temperature rise in the substrate is high for the variable thermal properties case than that of the constant properties case. The high temperature region extends along the axial direction in the symmetry axis where the absorbed laser power intensity is high. It should be noted that laser power intensity distribution at the substrate surface is Gaussian and the peak intensity occurs at the symmetry axis. Increase in the cavity depth because of constant properties case is almost twice of that corresponding to the variable thermal properties case during the heating pulse of 6 ns while it is only 1.35 times after 24 ns, which corresponds to the time of 15 ns after the laser pulse ends. Consequently, enhancement in the cavity depth is significant during the heating pulse and it slows progressing after the laser pulse ends. Moreover, increase in the cavity depth after the laser pulse ending is associated with the convection heating of the cavity surface by the vapor front present in the cavity. Three-dimensional view of the cavity shape is shown in Fig. 4 for variable and constant thermal properties case. Cavity enhancement in the axial direction is more pronounced than that of radial extension.

Fig. 5 shows temperature distribution along the symmetry axis inside the substrate material for constant as well as variable thermal properties cases at different heating durations. It should be noted that temperature is limited to the evaporation temperature of the substrate material along the temperature axis in the figure. Temperature decreases sharply in the liquid region ($T > T_m$) as compared to the solid region ($T < T_m$). The sharp decay of temperature can be related to the energy absorbed by the substrate material from the irradiated filed in this region. It should be noted that the laser absorbed energy decreases exponentially with the increasing depth below the surface (Lambert's law). In the solid region temperature decreases with increasing depth below the surface due to the diffusional energy transport in this region, since the solid region extends beyond the absorption depth. Consequently, contribution of irradiated energy to temperature rise in the solid region is not significant; therefore, temperature decay in this region depends on temperature gradient which is the only driving force for a diffusional heating in this region. As temperature gradient reduces with increasing depth from the liquid–solid interface, temperature decay becomes gradual due to small diffusional energy transfer in this region. The mushy zone developed between the liquid–solid phases is evident for the constant properties case (temperature remains constant at melting temperature at a short depth). Moreover, the depth of the cavity is deeper for the con-

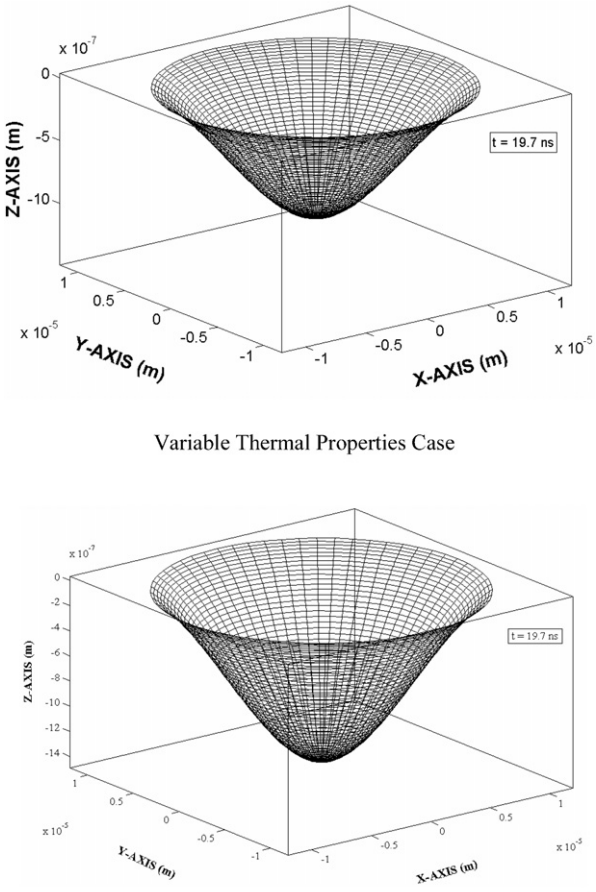

Fig. 4. Cavity shape obtained for variable and constant thermal properties case at 19.7 ns of heating duration.

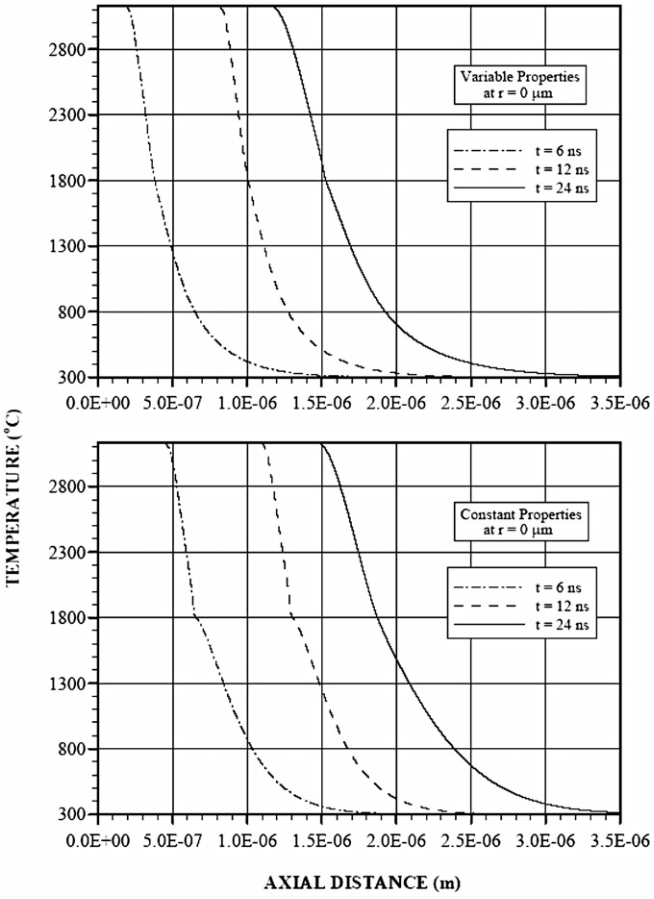

Fig. 5. Temperature distribution inside the substrate material along the symmetry axis obtained from variable and constant thermal properties cases for different heating durations.

stant properties case than the variable thermal properties case. This situation is also seen from Fig. 6, in which cross-sectional view of the heated regions is shown. This indicates that temperature dependent properties have significant effect on the melting and evaporation rates. In this case, thermal conductivity reduces with increasing temperature, which, in turn, results in small heat diffusion from the irradiated region to its neighborhood. However, increased specific heat capacity with temperature reduces temperature rise in the irradiated region suppressing the melting and evaporation rates in this region. Consequently, increasing specific heat capacity and reducing thermal conductivity with increasing temperature yield the small cavity depth for the variable thermal properties case. The small size of the liquid–solid mushy zone is associated with the low rate of heat diffusion from the liquid to the solid phases as well as low temperature rise in the liquid phase in the region next to the solid phase, i.e., reducing thermal conductivity with increasing temperature suppresses the diffusional energy transport from the liquid phase to the solid phase while increasing specific heat capacity with increasing temperature lowers temperature rise in the liquid region next to the solid phase.

Fig. 7 shows temperature distribution in the radial direction at the surface for constant and variable thermal properties cases at different durations. The extension of the cavity size, as judged by the radial distance corresponding to the evaporation temperature, is evident for constant properties case due to high heat rate of diffusion and high rise of temperature due to high thermal conductivity and low specific heat capacity. Moreover, convective cooling as well as energy diffusion from the surface region to the solid bulk after pulse ending results in decay of temperature in the radial direction. This situation can be observed when comparing temperature profiles at 12 ns and 24 ns heating durations, i.e., cooling of the surface results in the temperature profile to move towards the symmetry axis ($r = 0$) in the radial direction. The radial temperature gradient in the liquid phase is large for time period $t > 12$ ns, which corresponds to duration after the laser pulse ending. This is true for temperature profiles in the liquid and solid phases. Consequently, cooling of the surface results in sharp decay of temperature in both phases after the laser pulse ending. However, the size of mushy zone in the radial direction is larger than that of axial direction due to laser power intensity distribution in the radial direction at the surface, which is Gaussian. This situation is also observed from Fig. 2. In this case, laser power intensity at the surface reduces with increasing radial distance from the symmetry axis. This, in turn, enhances the size of the mushy zone in the radial direction.

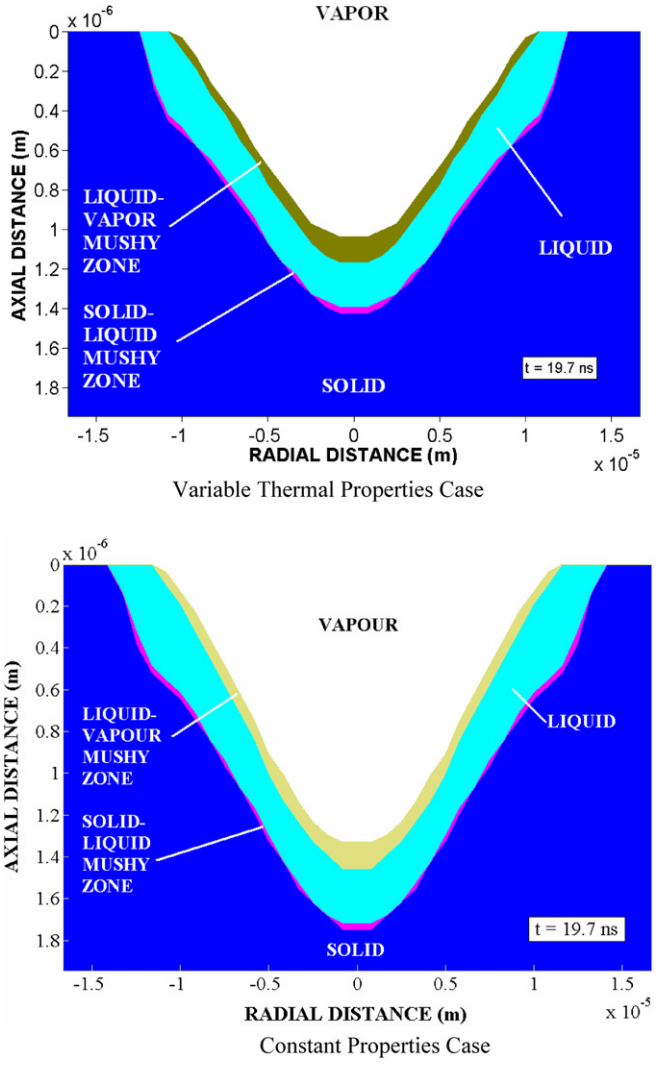

Fig. 6. Cavity cross sections obtained for variable and constant thermal properties cases.

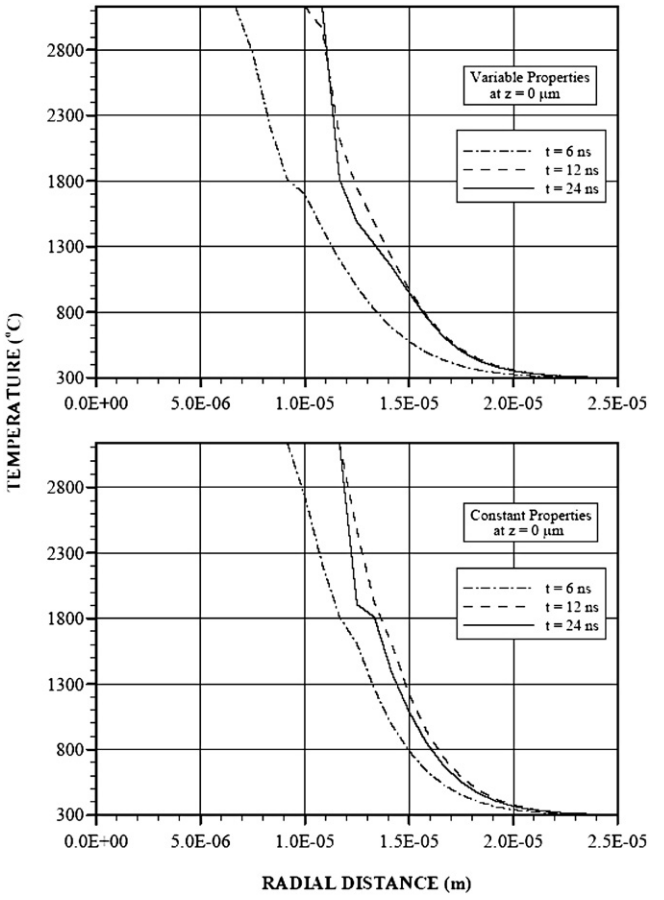

Fig. 7. Temperature distribution along the radial axis for variable and constant thermal properties cases.

Fig. 8 shows temporal variation of temperature at the symmetry axis at different depths below the surface for constant and variable thermal properties of the substrate material. In the case of constant properties, the rise of the temperature is rapid in the solid as well as in the liquid phases. This is more pronounced in the surface vicinity where the power intensity absorption is the highest. Increasing depth below the surface lowers the rise of temperature in both phases, in particular in the liquid phase. This is associated with the amount of absorbed radiated energy by the substrate material, which reduces with increasing depth from the surface (Lambert's law). Moreover, the duration of constant melting temperature remains almost the same at different depths below the surface. This indicates that the duration of mushy zone formation in the substrate material remains almost constant with increasing depth, provided that the recession of the mushy zone in to the substrate material may not be constant, since the time required for melting changes in a nonlinearly form as the depth below the surface increases. When comparing constant and variable thermal properties cases, temperature rise is slower in both phases for the variable thermal properties. This is more pronounced with increasing depth below the surface. The slow rise of temperature at the surface, despite reducing thermal conductivity with increasing temperature, is because of the increase of the specific heat capacity with temperature. In this case, reducing thermal conductivity with increasing temperature results in less energy dissipation from the irradiated surface towards the solid bulk, i.e., temperature is expected to rise in the surface region. However, increasing specific heat capacity with increasing temperature suppresses temperature rise in the surface region. Consequently, large increase in the specific heat capacity with increasing temperature lowers temperature rise in the surface region despite the decrease in thermal conductivity. It should be noted that the magnitude of decrease in thermal conductivity between 100 °C and 1500 °C is 101.9 W/m K while the magnitude of increase in specific heat capacity between 100 °C and 1500 °C is 438 J/kg K. Therefore, large magnitude of increase in specific heat capacity is response for slow rise in temperature in the surface region. Moreover, the slow rise of temperature in the solid phase in the region close to the melting temperature as well as the in the liquid phase close to the vapor temperature is because of the mushy zones formed across the liquid–solid and vapor–liquid phases. Therefore, the mushy zones act like a heat sink at the inter-phases lowering the temperature rise in the inter-phase vicinity.

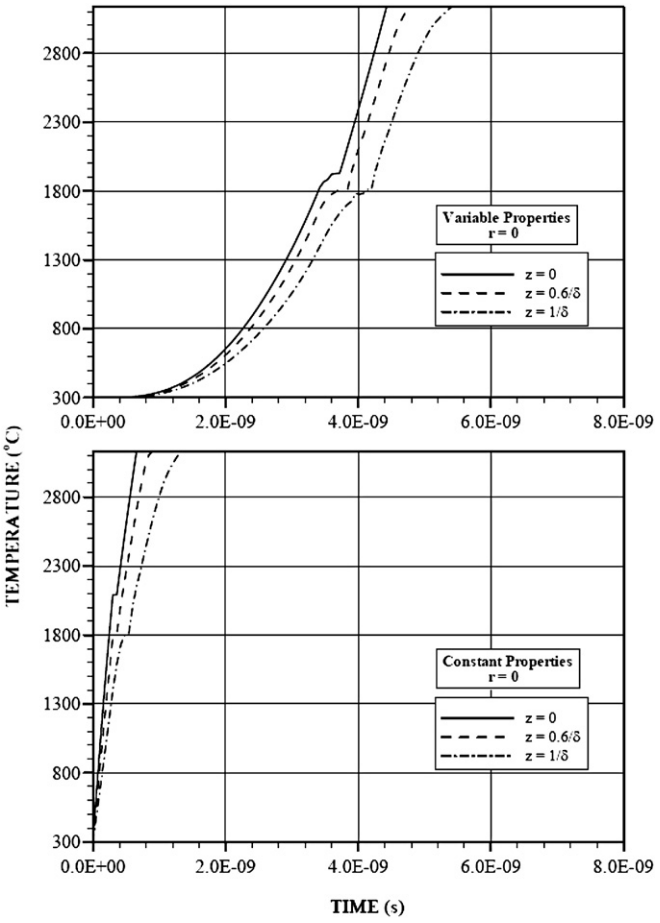

Fig. 8. Temporal variation of temperature obtained for variable and constant thermal properties cases.

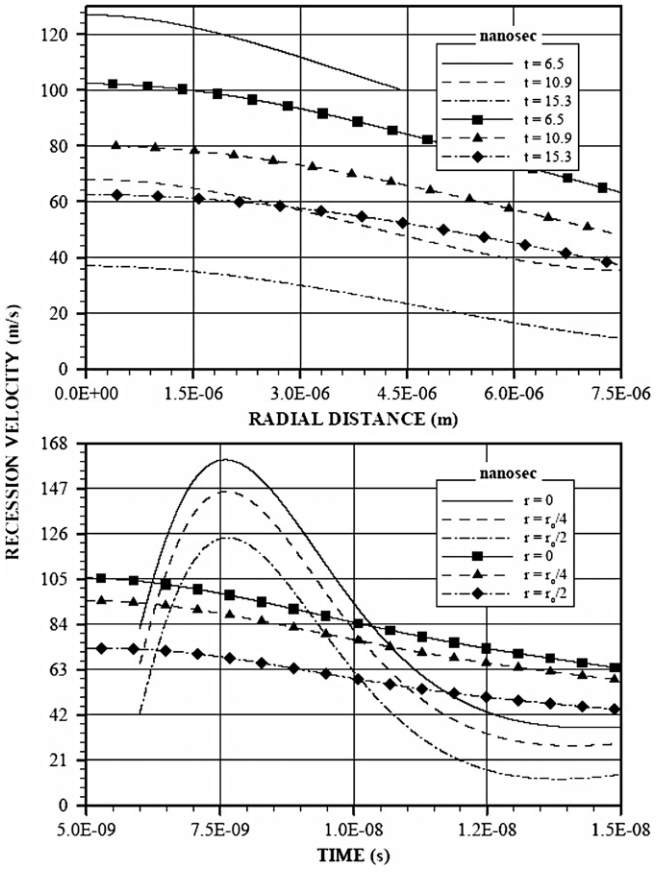

Fig. 9. Recession velocity variation along the radial direction and with time obtained for variable and constant thermal properties cases.

Fig. 9 shows recession velocity of the vapor–liquid surface along the radial direction for different heating periods. Recession velocity is higher along the symmetry axis and it reduces gradually with increasing radial distance from the symmetry axis. Recession of the liquid–solid surface towards the solid bulk is higher in the case of variable thermal properties cases than that of constant properties case. This is true for heating periods $t \leqslant 10.9$ ns. The attainment of the high recession velocity for variable thermal properties case is because of the small energy diffusion in the irradiated region due to low thermal conductivity at high temperatures. However, once the laser pulse intensity reduces significantly, it also reduces significantly. In the case of variable thermal properties case, low thermal conductivity at high temperatures results in higher recession velocity than that of constant properties case in the cooling cycle ($t = 15.3$ ns). Consequently, once the laser pulse intensity reduces, recession velocity decreases for variable thermal properties case. However, the decrease in recession velocity results in small cavity depth because of small rate of evaporation from the surface. In the case of temporal variation of recession velocity at different radial locations for constant and variable thermal properties case (Fig. 9). Recession velocity initiates earlier for the constant properties case because of the early start of evaporation. In the case of variable thermal properties case, recession velocity increases rapidly and reaches its maximum, and then decays rapidly with progressing time. High recession velocity occurs during the period of 6–10 ns, when the laser power intensity is high. As the power intensity reduces with the progressing time so that the recession velocity reduces. When comparing recession velocity due to constant and variable thermal properties cases, recession velocity corresponding to the variable thermal properties case attains higher values than that of constant properties case during the time period of 6–10 ns. This is because of increasing specific heat capacity with temperature, which in turn increases the internal energy gain of the substrate material at vapor temperature. This accelerates the rate of operation at the surface. Moreover, small conductivity at high temperatures suppresses the thermal diffusion from the irradiated region to the solid bulk. This contributes to the enhancement of internal energy gain in the surface region. Consequently, evaporation rate increases further so that recession velocity increases. Fig. 10 shows comparison of recession velocity predicted from variable and constant thermal properties cases and obtained from the previous analytical solution [19]. When comparing recession velocities, it can be observed that recession velocity predicted for the constant properties case agrees well with the result of the analytical solution. It should be noted that analytical solution is obtained for the constant properties case. Moreover, some small discrepancies between the result of analytical solution and the predictions are because of the one-dimensional consideration in the analytical solution.

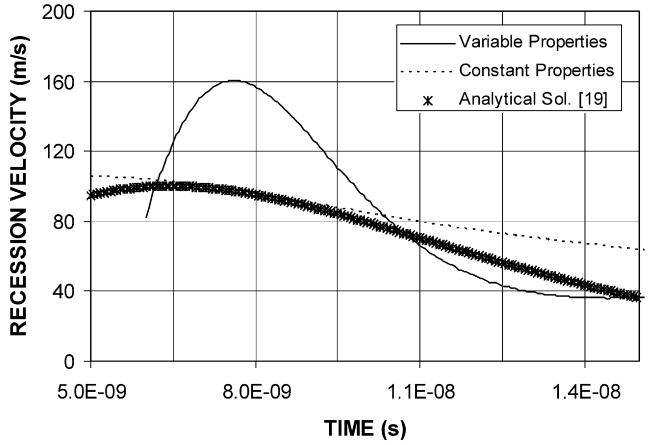

Fig. 10. Comparison of recession velocity obtained from present predictions along the symmetry axis for variable and constant thermal properties cases and one-dimensional analytical solution [19].

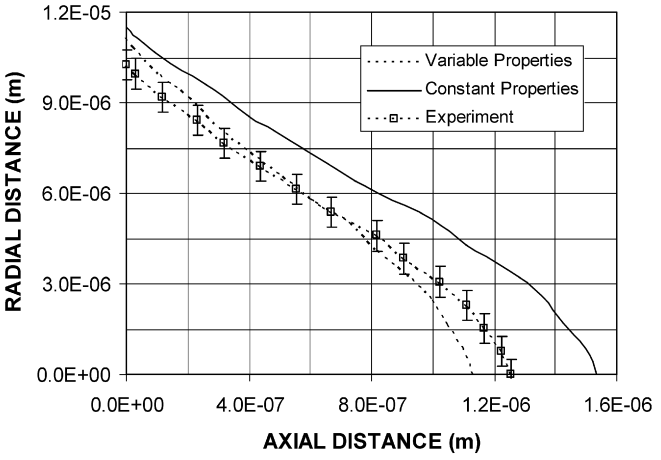

Fig. 11. Cavity profiles predicted from variable and constant thermal properties cases and the experiment.

Fig. 11 shows cavity shape predicted from the variable and constant thermal properties cases as well as obtained from the experiment. It can be observed that cavity is obtained from the variable thermal properties case agrees well with the experimental results.

5. Conclusions

Laser pulse heating and cavity formation in the irradiated region are examined. Temperature rise in the substrate material and formation of the mushy zones across the liquid–solid and liquid–vapor phases are formulated. Laser pulse shape resembling the laser actual pulse is accommodated in the analysis. The constant and variable thermal properties of steel are considered in the simulations and temperature predictions are compared. An experiment is conducted to compare the cavity shape predicted for constant and variable thermal properties cases. The closed form solution developed in the early study for recession velocity is accommodated to compare the predictions with the results of analytical solution. It is found that variable thermal properties case results in shallower cavity depth than that of constant properties case, particularly along the symmetry axis where the laser power intensity is the highest. In this case, increasing specific heat capacity with temperature is responsible for the shallow cavity depth despite reducing thermal conductivity with increasing temperature. Rise of temperature in the solid and liquid phases is larger for constant properties case than that corresponding to the variable thermal properties case. The evaporation of the surface starts earlier for the constant properties case than that of the variable thermal properties case. This, in turn, enhances the cavity depth along the symmetry axis. Recession velocity attains high for the variable thermal properties case during the time when the laser pulse intensity reaches its maximum. However, as the heating duration progresses, recession velocity for the constant properties case becomes higher than that corresponding to the variable thermal properties. When comparing recession velocity obtained from the analytical solution and the present predictions, prediction corresponding to the constant properties agrees well with the result of analytical solution, since the analytical solution is obtained for the constant properties. Moreover, when the depth of cavity obtained from the experiment and predicted from the simulations are compared, prediction of variable thermal properties case agrees well with the experimental result.

Acknowledgements

The authors acknowledge the support of King Fahd University of Petroleum and Minerals. Dhahran, Saudi Arabia for this work.

Appendix A. Discretization of the governing equations

The relevant governing equations are Eqs. (1), (3), (5), and (6). These equations contain four main variables, T_s, T_l, x_m and x_b. In actual numerical implementation we treat T_s and T_l as the same variable since solid and liquid do not exist simultaneously at a grid point. Where they do, they are described by means of the quality. So we need to discretized only three equations. These equations contain the following generic derivative terms, $\frac{\partial T}{\partial t}$, $\frac{1}{r}\frac{\partial}{\partial r}(r\frac{\partial T}{\partial r})$, $\frac{\partial^2 T}{\partial z^2}$ and $\frac{\partial x}{\partial t}$. For a grid point C, E and W are its r-direction neighbors, while N and S are its z-direction neighbors as shown in Fig. A.1. For temporal derivatives first-order backward differences are used whereas for spatial derivatives second-order central differences have been employed. These selections lead to an implicit scheme.

If we set p as the time index, i as the r-coordinate index and j as the z-coordinate index then the discretized form of Eq. (1) becomes:

$$a_C T^p_{i,j} = a_E T^p_{i+1,j} + a_W T^p_{i-1,j} + a_N T^p_{i,j+1} + a_S T^p_{i,j-1} + T^{p-1}_{i,j} + a_H S^p_{i,j} \quad (A.1)$$

where

$$a_E = \frac{\alpha \Delta t (r_i + 0.5\Delta r)}{r_i (\Delta r)^2}, \quad a_W = \frac{\alpha \Delta t (r_i - 0.5\Delta r)}{r_i (\Delta r)^2}$$

$$a_N = a_S = \frac{\alpha \Delta t}{(\Delta z)^2}, \quad a_H = \frac{\Delta t}{\rho C p}$$

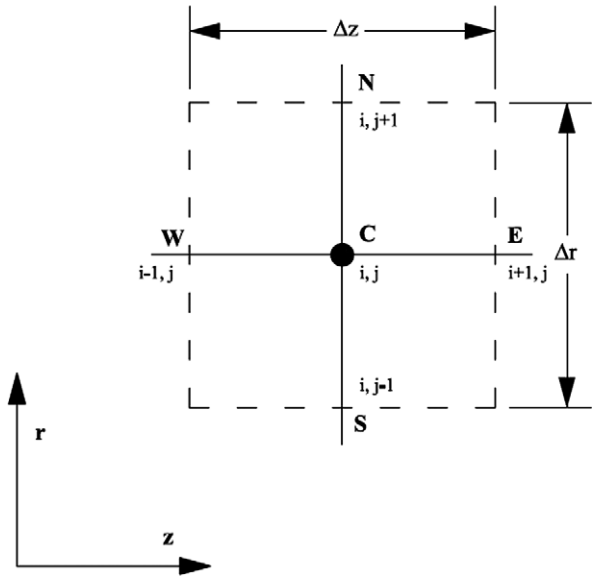

Fig. A.1. An internal grid point with neighbors for an axisymmetric laser heating of a substrate material.

$$a_C = 1 + a_E + a_W + a_N + a_S$$

In the case of solid phase:

$$\rho = \rho_s, \quad Cp = Cp_s(T), \quad \alpha = \frac{k_s(T)}{\rho_s Cp_s(T)}$$

In the case of liquid phase:

$$\rho = \rho_l, \quad Cp = Cp_l(T), \quad \alpha = \frac{k_l(T)}{\rho_l Cp_l(T)}$$

The discretize form of the equation determining the quality (x_m) in the solid–liquid mushy zone yields:

$$x^p_{m_{i,j}} = b_E T^p_{i+1,j} - b_C T^p_{i,j} + b_W T^p_{i-1,j} + b_Z\left(T^p_{i,j+1} - 2T^p_{i,j} + T^p_{i,j-1}\right) + b_H S^p_{i,j} + x^{p-1}_{m_{i,j}} \quad \text{(A.2)}$$

where

$$b_E = \frac{\alpha_m Cp_m \Delta t (r_i + 0.5\Delta r)}{L_m r_i (\Delta r)^2}, \quad b_W = \frac{\alpha_m Cp_m \Delta t (r_i - 0.5\Delta r)}{L_m r_i (\Delta r)^2}$$

$$b_C = b_E + b_W, \quad b_N = b_S = \frac{\alpha_m Cp_m \Delta t}{L_m (\Delta z)^2}, \quad b_H = \frac{\Delta t}{\rho_m L_m}$$

The discretize form of the equation determining the quality (x_b) in the liquid–vapor mushy zone yields:

$$x^p_{b_{i,j}} = c_E T^p_{i+1,j} - c_C T^p_{i,j} + c_W T^p_{i-1,j} + c_Z\left(T^p_{i,j+1} - 2T^p_{i,j} + T^p_{i,j-1}\right) + c_H S^p_{i,j} + x^{p-1}_{b_{i,j}} \quad \text{(A.3)}$$

where

$$c_E = \frac{\alpha_b Cp_b \Delta t (r_i + 0.5\Delta r)}{L_b r_i (\Delta r)^2}, \quad c_W = \frac{\alpha_b Cp_b \Delta t (r_i - 0.5\Delta r)}{L_b r_i (\Delta r)^2}$$

$$c_C = c_E + c_W, \quad c_N = c_S = \frac{\alpha_b Cp_b \Delta t}{L_b (\Delta z)^2}, \quad b_H = \frac{\Delta t}{\rho_b L_b}$$

For all equations,

$$S^p_{i,j} = I_o(t)\delta(1 - r_f)\exp(-\delta z_j)\exp\left(-r_i^2/a^2\right) \quad \text{(A.4)}$$

During the laser heating of the substrate it is to be noted that when evaporation starts, the metal vapor is ejected out and leaves behind a cavity. The laser beam is now focused on the deformed surface of the substrate, which constitutes the cavity. This aspect has to be accommodated in the solution procedure. In this case the heat source distribution has to be modified so that its peak value always occurs at the substrate surface. The appropriate modifications are,

$$S^p_{i,j} = I_o(t)\delta(1 - r_f)\exp\left(-\delta(z_j - zc_i)\right)\exp\left(-r_i^2/a^2\right) \quad (0 \leqslant r \leqslant r_{\max},\ z \geqslant zc_i)$$

$$S^p_{i,j} = I_o(t)\delta(1 - r_f)\exp(-\delta z_j)\exp\left(-r_i^2/a^2\right) \quad (r > r_{\max})$$

where zc_i is the depth of the cavity, which varies with r_i until $r = r_{\max}$ where $zc = 0$.

References

[1] M. Kalyon, B.S. Yilbas, Analytical solution for laser evaporative heating process: time exponentially decaying pulse case, J. Phys. D: Appl. Phys. 34 (2001) 3303–3311.

[2] B.S. Yilbas, S.Z. Shuja, Laser non-conduction limited heating and prediction of surface recession velocity in relation to drilling, Proc. Inst. Mech. Eng., Part C: J. Mech. Engrg. Sci. 217 (2003) 1067–1076.

[3] B.S. Yilbas, Laser heating process and experimental validation, Int. J. Heat Mass Transfer 40 (1997) 1131–1143.

[4] R.K. Ganesh, A. Faghri, Y. Hahn, A generalized thermal modeling for laser drilling process – I. Mathematical modeling and numerical methodology, Int. J. Heat Mass Transfer 40 (1997) 3351–3360.

[5] W. Pecharapa, A. Kar, Effects of phase changes on weld pool shape in laser welding, J. Phys. D: Appl. Phys. 30 (1997) 3322–3329.

[6] C.L. Liu, J.N. Leboeuf, R.F. Wood, D.B. Geobegan, J.M. Donato, K.R. Chen, A.A. Puretzky, Computational modeling of physical processes during laser ablation, Mater. Sci. Engrg. B: Solid-State Materials for Advanced Technology B47 (1997) 70–77.

[7] P. Solana, P. Kapadia, J.M. Dowden, P.J. Marsden, An analytical model for the laser drilling of metals with absorption within the vapor, J. Phys. D: Appl. Phys. 32 (1999) 942–952.

[8] A.V. Gusarov, A.G. Gnedovets, I. Smurov, Two-dimensional gas-dynamic model of laser ablation in an ambient gas, Appl. Surface Sci. 154 (2000) 66–72.

[9] W. Kim, B. Sim, Study of thermal behavior and fluid flow during laser surface heating of alloys, Numer. Heat Transfer, Part A 31 (1997) 703–723.

[10] A. Rostami, A. Raisi, Temperature distribution and melt pool size in a semi-infinite body due to a moving laser heat source, Numer. Heat Transfer, Part A 31 (1997) 783–796.

[11] A. Matsunawa, V. Semak, The simulation of front keyhole wall dynamics during laser welding, J. Phys. D: Appl. Phys. 30 (1997) 798–809.

[12] Y. Zhang, A. Faghri, Vaporization, melting and heat conduction in the laser drilling process, Int. J. Heat Mass Transfer 42 (1999) 1775–1790.

[13] B. Basu, A.W. Date, Numerical study of steady state and transient laser melting problems – I. Characteristics of flow field and heat transfer, Int. J. Heat Mass Transfer 33 (6) (1990) 1149–1163.

[14] Z.H. Shen, S.Y. Zhang, J. Lu, X.W. Ni, Mathematical modeling of laser induced heating and melting in solids, Optics and Laser Technology 33 (2001) 533–537.

[15] S. Safdar, L. Lin, M.A. Sheikh, Numerical analysis of the effects of non-conventional laser beam geometries during laser melting of metallic materials, J. Phys. D: Appl. Phys. 40 (2007) 593–603.

[16] D. Chatterjee, S. Chakraborty, An enthalpy-based lattice Boltzmann model for diffusion dominated solid–liquid phase transformation, Phys. Lett. A 341 (2005) 320–330.

[17] B.S. Yilbas, S.B. Mansour, Laser heating: jet emanating from laser induced cavity, Int. J. Thermal Sci. 46 (4) (2007) 385–398.

[18] B.S. Yilbas, S.B. Mansoor, Laser evaporative heating of surface: Simulation of flow field in the laser produced cavity, J. Phys. D: Appl. Phys. 39 (17) (2006) 3863–3875.
[19] M. Kalyon, B.S. Yilbas, Analytical solution for laser evaporative heating process: time exponentially decaying pulse case, J. Phys. Part D: Appl. Phys. 34 (2001) 3303–3311.
[20] S.V. Patankar, Numerical Heat Transfer, McGraw-Hill, New York, 1980.
[21] I.Z. Naqavi, Conduction and non-conduction limited laser heating process – mathematical simulation, M.Sc. Thesis, Mech. Eng. Dept., KFUPM, 2001.